Modulation of L-Type Ca^{2+} Channels by Distinct Domains Within SNAP-25

Junzhi Ji,[1] Shao-Nian Yang,[2] Xiaohang Huang,[1] Xidan Li,[2] Laura Sheu,[1] Nicholas Diamant,[1,3] Per-Olof Berggren,[2] and Herbert Y. Gaisano[1,3]

Cognate soluble *N*-ethylmaleimide–sensitive factor attachment protein receptor (SNARE) proteins are now known to associate the secretory vesicle with both the target plasma membrane and Ca^{2+} channels in order to mediate the sequence of events leading to exocytosis in neurons and neuroendocrine cells. Neuroendocrine cells, particularly insulin-secreting islet β-cells, t-SNARE proteins, 25-kDa synaptosomal-associated protein (SNAP-25), and syntaxin 1A, independently inhibit the L-type Ca^{2+} channel (L_{Ca}). However, when both are present, they actually exhibit stimulatory actions on the L_{Ca}. This suggests that the positive regulation of the L_{Ca} is conferred by a multi-SNARE protein complex. We hypothesized an alternate explanation, which is that each of these SNARE proteins possess distinct inhibitory and stimulatory domains that act on the L_{Ca}. These SNARE proteins were recently shown to bind the $Lc_{753–893}$ domain corresponding to the II and III intracellular loop of the α1C subunit of the L_{Ca}. In this study, using patch-clamp methods on primary pancreatic β-cells and insulinoma HIT-T15 cells, we examined the functional interactions of the botulinum neurotoxin A (BoNT/A) cleavage products of SNAP-25, including NH_2-terminal (1–197 amino acids) and COOH-terminal (amino acid 198–206) domains, on the L_{Ca}, particularly at the $Lc_{753–893}$ domain. Intracellular application of SNAP-$25_{1–206}$ in primary β-cells decreased L_{Ca} currents by ~15%. The reduction in L_{Ca} currents was counteracted by coapplication of $Lc_{753–893}$. Overexpression or injection of wild-type SNAP-25 in HIT cells reduced L_{Ca} currents by ~30%, and this inhibition was also blocked by the recombinant $Lc_{753–893}$ peptide. Expression of BoNT/A surprisingly caused an even greater reduction of L_{Ca} currents (by 41%), suggesting that the BoNT/A cleavage products of SNAP-25 might possess distinct inhibitory and positive regulatory domains. Indeed, expression of SNAP-$25_{1–197}$ increased L_{Ca} currents (by 19% at 10 mV), and these effects were blocked by the $Lc_{753–893}$ peptide. In contrast, injection of SNAP-$25_{198–206}$ peptide into untransfected cells inhibited L_{Ca} currents (by 47%), and more remarkably, these inhibitory effects dominated over the stimulatory effects of SNAP-$25_{1–197}$ overexpression (by 34%). Therefore, the SNARE protein SNAP-25 possesses distinct inhibitory and stimulatory domains that act on the L_{Ca}. The COOH-terminal 197–206 domain of SNAP-25, whose inhibitory actions dominate over the opposing stimulatory NH_2-terminal domain, likely confers the inhibitory actions of SNAP-25 on the L_{Ca}. We postulate that the eventual accelerated proteolysis of SNAP-25 brought about by BoNT/A cleavage allows the relatively intact NH_2-terminal SNAP-25 domain to assert its stimulatory action on the L_{Ca} to increase Ca^{2+} influx, and this could in part explain the observed weak or inconsistent inhibitory effects of BoNT/A on insulin secretion. The present study suggests that distinct domains within SNAP-25 modulate L_C subtype Ca^{2+} channel activity in both primary β-cells and insulinoma HIT-T15 cells. *Diabetes* 51:1425–1436, 2002

In pancreatic islet β-cells, insulin exocytosis involves an intimate and sequential relationship between the Ca^{2+} influx via plasma membrane Ca^{2+} channels and the exocytotic fusion machinery. However, dysregulation of Ca^{2+} influx across the Ca^{2+} channels has been postulated as a mechanism of islet β-cell death caused by an undefined serum factor in patients with type 1 diabetes (1) as well as during treatment with sulfonylureas (2) and exposure to cytokines (3). It therefore is important to identify the precise molecules and their domains that bind and regulate the islet β-cell Ca^{2+} channels.

Soluble *N*-ethylmaleimide–sensitive factor attachment protein receptor (SNARE) proteins that mediate fusion of these synaptic and hormone-containing vesicles are also capable of directly binding and modulating the Ca^{2+} channels (4–6). In the pancreatic islet β-cells, an excellent neuroendocrine cell model for study of the SNARE/Ca^{2+} channel interactions, the L-type Ca^{2+}channel (L_{Ca}) and Ca^{2+} influx, was found to be colocalized to the sites of insulin granule exocytosis (7). In this regard, Wiser et al. (8) reported that the t-SNAREs syntaxin 1A and 25-kDa synaptosomal-associated protein (SNAP-25); and the v-SNARE synaptotagmin bind the cytoplasmic domain ($Lc_{753–893}$) of the II-III L-loop of the α1c subunit of L-type C-class, which is common to the neuronal N-type Ca^{2+} channel. They further showed that injection of this $Lc_{753–893}$ peptide disrupted depolarization-evoked insulin secretion but not L_{Ca} activity per se; and that syntaxin 1A inhibition of L_{Ca} activity could be reversed by coexpression of synaptotagmin. These functional results led these

From the [1]Department of Medicine, University of Toronto, Toronto, Canada; [2]The Rolf Luft Center for Diabetes Research, Department of Molecular Medicine, Karolinska Institutet, Karolinska Hospital, Stockholm, Sweden, and the [3]Department of Physiology, University of Toronto, Toronto, Canada.

Address correspondence and reprint requests to Dr. Herbert Y. Gaisano, Room 7226 Medical Sciences Building, University of Toronto, 1 King's College Circle, Toronto, Ontario, Canada M5S 1A8. E-mail: herbert.gaisano@utoronto.ca.

Received for publication 1 May 2001 and accepted in revised form 11 February 2002.

BoNT/A, botulinum neurotoxin A; $[Ca^{2+}]_i$, cytoplasmic-free Ca^{2+} concentration; GFP, green fluorescence protein; GST, glutathione S-transferase; L_{Ca}, L-type Ca^{2+} channel; SNAP-25, 25-kDa synaptosomal-associated protein; SNARE, soluble *N*-ethylmaleimide–sensitive factor attachment protein receptor; TEA, tetraethylamonium.

workers to postulate that in the basal state, syntaxin 1A binds and inhibits the L_{Ca} and that during stimulation, synaptotagmin associated with the approaching insulin granule binds syntaxin 1A, forming a complex of the vesicle with the L_{Ca}, termed an excitosome (8). With this binding, synaptotagmin would then prevent syntaxin 1A inhibition of the L_{Ca}, thereby allowing Ca^{2+} entry to occur at the site of exocytosis (8).

Despite progress in examining the structure/function of SNARE proteins in membrane fusion (9), the precise molecular interactions between these SNARE proteins and Ca^{2+} channels are only now becoming clearer, particularly through the use of clostridial neurotoxins that specifically cleave SNARE proteins (10). Early studies have shown that tetanus toxin, which cleaves VAMP and botulinum toxins A and C1 (which cleave SNAP-25 and syntaxin 1A), inhibit neurotransmitter and insulin release (11–14), but the inhibition by botulinum neurotoxin A (BoNT/A) could be reversed by an increasing extracellular Ca^{2+} (13,15). Intuitively, the increased Ca^{2+} influx observed in BoNT/A-treated chromaffin cells raises the possibility that cleavage products of the substrate by BoNT/A might directly affect Ca^{2+} influx, perhaps by actions on the Ca^{2+} channels.

In this work, we have demonstrated the modulation of L_C subtype Ca^{2+} channel activity by full-length SNAP-25 in primary pancreatic β-cells and then used the neuroendocrine model, insulinoma HIT-T15 cells, to further examine the effects of BoNT/A cleavage products of SNAP-25, including NH_2-terminal 1–197 amino acid and COOH-terminal amino acid 198–206, on the L_{Ca}. HIT cells reliably and uniformly take up multiple plasmids, including one containing the green fluorescence proteins (GFPs) that identify the transfected cells for patch-clamp studies (16). This capability has allowed us to identify the cells expressing the NH_2-terminal truncated SNAP-$25_{1–197}$ protein with or without injection of the SNAP-$25_{198–206}$ peptide. Surprisingly, we found that NH_2-terminal SNAP-$25_{1–197}$ possesses a positive regulatory action on the L_{Ca}, explaining the previously observed increased Ca^{2+} influx in BoNT/A-treated cells. The stimulatory action of SNAP-$25_{1–197}$ on the L_{Ca} opposes its inhibitory effects on exocytotic fusion (15). In contrast, the COOH-terminal SNAP-$25_{198–206}$ potently inhibited L_{Ca} activity and overcame the stimulatory effects of the SNAP-$25_{1–197}$ domain. This COOH-terminal region therefore confers the inhibitory effect of full-length SNAP-25 on the L_{Ca}. Blockade of SNAP-$25_{1–197}$ effects on the L_{Ca} by the $Lc_{753–893}$ domain of the channel further indicates the specific interactions of these protein domains.

RESEARCH DESIGN AND METHODS

Primary pancreatic β-cell culture. Islets of Langerhans were isolated from mice and dispersed into single cells that were then grown in RPMI-1640 medium (Gibco, Middlesex, UK).

Cell culture and transfections. HIT-T15 cells were grown at 37°C in 5% CO_2/95% air in RPMI-1640 medium supplemented with 20 mmol/l glutamine, 10% FCS (Gibco, Gaithersburg, MD), penicillin (100 units/ml), and streptomycin (100 mg/ml). When the cells were confluent, they were passaged and transiently transfected with 2 mg empty plasmid vector (control) or plasmid DNA encoding for SNAP-$25_{1–206}$, BoNT/A light chain, or SNAP-$25_{1–197}$ (16). The transfection of plasmid DNA was facilitated using Pfx-1 lipid (Invitrogen, Carlsbad, CA) at a ratio of 1:6 (wt/wt). After a 4-h incubation at 37°C in 5% CO_2/95% air, normal RPMI-1640 medium was replaced. Transfection efficiency was determined by using pcDNA3/His/Lac Z (Invitrogen) as a control plasmid for transfections, followed by determination of β-galactosidase expression. In a previous study (16), HT-T15 cells were found to uniformly intake the plasmids. Therefore, successfully transfected cells were confirmed by coexpression and visualization of the GFPs (Clontech, Palo, CA).

Whole-cell patch-clamp studies. Whole-cell Ca^{2+} currents were recorded in pancreatic β-cells from adult male and female mice. Pipettes were pulled from borosilicate glass capillaries (Hilgenberg, Malsfeld, Germany) on a horizontal programmable puller (DMZ Universal Puller; Zeitz-Instrumente, Augsburg, Germany). Typical electrode resistance was 3–5 MΩ. Electrodes were filled with a standard internal solution containing glutathione S-transferase (GST) (10^{-9} mol/l), GST SNAP-$25_{1–206}$ (10^{-9} mol/l), $Lc_{753–893}$ (10^{-6} mol/l), or $Lc_{753–893}$ (10^{-6} mol/l) combined with GST SNAP-$25_{1–206}$ (10^{-9} mol/l). The standard internal solution contained the following (in mmol/l): 150.0 *N*-methyl-D-glucamine, 10.0 EGTA, 1.0 $MgCl_2$, 2.0 $CaCl_2$, 5.0 HEPES, and 3.0 Mg ATP (pH 7.2 adjusted with HCl). The cells were bathed in a solution containing the following (in mmol/l): 138.0 NaCl, 5.6 KCl, 1.2 $MgCl_2$, 10.0 $CaCl_2$, 5.0 HEPES, and 10.0 tetraethylamonium (TEA) (pH 7.4 adjusted with NaOH). After obtaining a seal, the holding potential was set at −70 mV during the experiment, and depolarizing voltage pulses (70 mV, 100 ms, 0.05 Hz) were applied. The resulting currents were recorded with an Axopatch 200 amplifier (Axon Instruments, Foster City, CA). All recordings were made at room temperature (~22°C). The amplitude of whole-cell Ca^{2+} currents was normalized by the cell capacitance. Acquisition and analysis of data were done using the software program pCLAMP (Axon Instruments).

On the third day after the transient transfection, the HIT-T15 cells were trypsinized and dispersed into single cells for patch-clamp study. Drops of medium containing these cells were placed in a 1-ml chamber mounted on the stage of an inverted phase-contrast microscope and allowed to stick to the bottom for 10 min. The RPMI-1640 medium was replaced by external solution composed of (in mmol/l): 20.0 $BaCl_2$, 90.0 NaCl, 5.0 CsCl, 1.0 $MgCl_2$, 20.0 TEA-Cl, and 10.0 HEPES (pH 7.4). Whole-cell configuration of the patch-clamp technique was applied to record membrane currents in single HIT-T15 cells, which showed GFP brightness under ultraviolet light. The pipette solution contained the following components (in mmol/l): 70.0 cesium aspartate, 1.0 $MgCl_2$, 5.0 EGTA, 4.0 Mg-ATP, and 20.0 HEPES (pH 7.2). Recordings were performed using an Axopatch 1D amplifier (Axon Instruments). Whole-cell voltage-clamp protocols were generated by pCLAMP6 software (Axon Instruments). All signals were filtered at 1 kHz by an on-board eight-pole Bessel filter before digitization with a Digiata 1200 analog-to-digital converter (Axon Instruments). Cell capacitance was determined by integration of the capacity transient. Data were presented as means ± SE and compared by unpaired Student's *t* test for single comparisons and by ANOVA for multiple comparisons. $P < 0.05$ was considered statistically significant. All experiments were performed at room temperature.

Intracellular Ca^{2+} measurement. HIT-T15 cells with different transfectants were cultured on coverslips. On the third day after transfection, the coverslips were placed in a 1-ml chamber and loaded with low Ca^{2+}-HEPES buffer solution containing 4 μmol/l Fura 2-AM (Molecular Probes, Eugene, OR) at room temperature for 45 min. Cells were then rinsed three times with a standard extracellular solution containing (in mmol/l) 125.0 NaCl, 5.0 KCl, 1.8 $CaCl_2$, 2.0 $MgCl_2$, 0.5 NaH_2PO_4, 5.0 $NaHCO_3$, 10.0 HEPES, and 10.0 glucose (pH 7.2). Single-cell Ca^{2+} imaging was performed at room temperature using a Merlin imaging system (Life Sciences Resources, Cambridge, UK). Fura 2-AM fluorescence was calibrated to Ca^{2+} concentration with 10 μmol/l ionomycin in the presence of 5 mmol/l $CaCl_2$ for maximal fluorescence ratio or with no added Ca^{2+} and 10 mmol/l EGTA for minimal fluorescence ratio (17). Cells with successful transfection were determined by concomitant transfection of GFP, which was illuminated with light at 470 nm. Two measures were taken to minimize the possible influence of GFP on fluorescence density from Fura 2. First, control cells were also transfected with GFP, as we did in electrophysiologic studies. Second, we only examined the cells with just-visible GFP fluorescence and eliminated those with maximal GFP fluorescent brightness at 470 nm to minimize optical interference.

RESULTS

Effect of GST SNAP-$25_{1–206}$ on voltage-gated Ca^{2+} currents in primary pancreatic β-cells. To test for possible modulation of voltage-gated Ca^{2+} currents by SNAP-25, pancreatic β-cells were dialyzed with GST (10^{-9} mol/l, control), GST SNAP-$25_{1–206}$ (10^{-9} mol/l), $Lc_{753–893}$ (10^{-6} mol/l) alone, or $Lc_{753–893}$ (10^{-6} mol/l) together with GST SNAP-$25_{1–206}$ (10^{-9} mol/l) through the recording pipette. Whole-cell voltage-gated Ca^{2+} currents from cells subjected to different treatments were evoked by step-depolarizing voltage pulses from a holding potential of

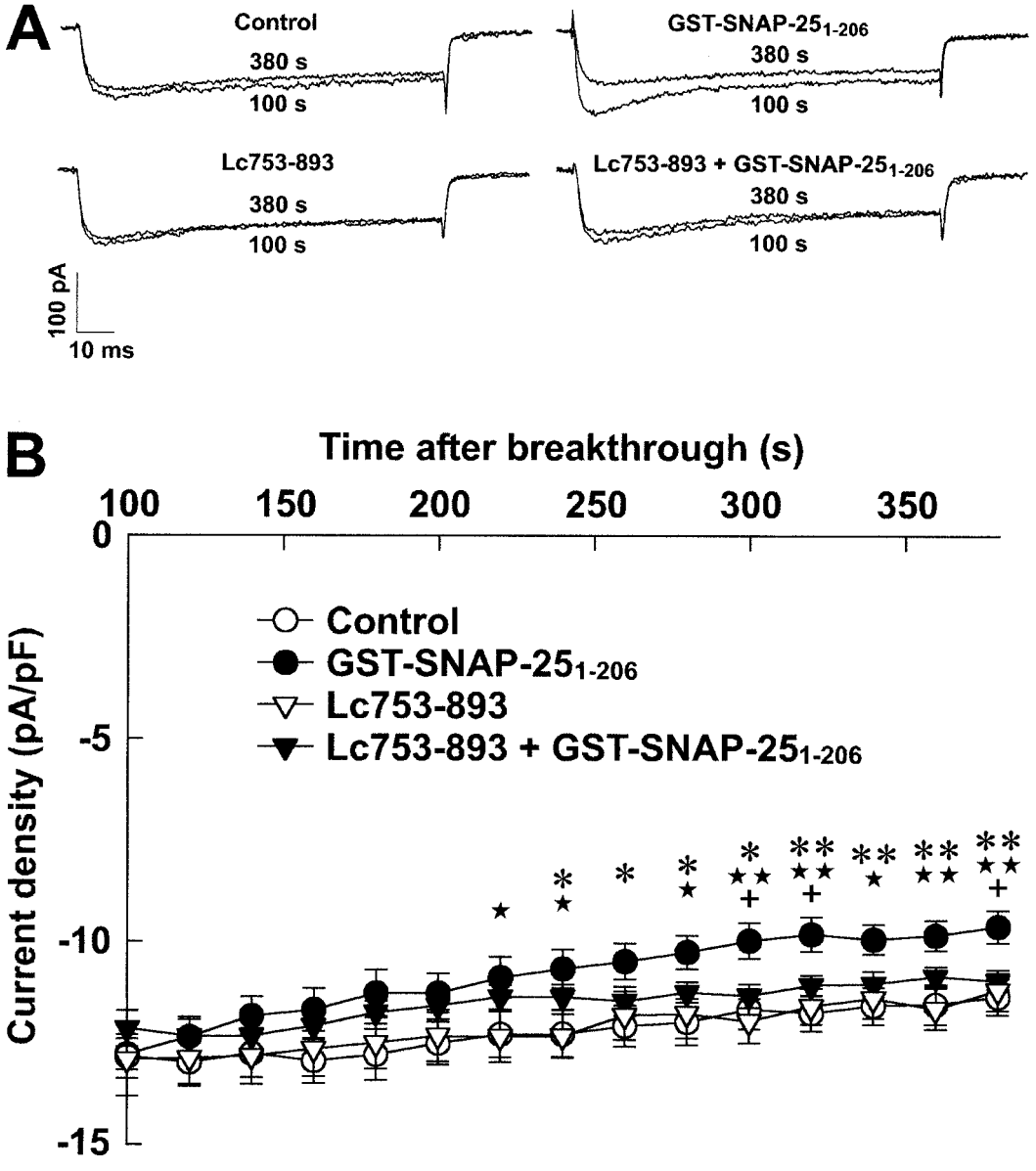

FIG. 1. Effect of GST-SNAP-25$_{1-206}$ on voltage-gated Ca^{2+} currents in the pancreatic β-cell. *A*: Cells dialyzed with GST as control, Lc$_{753-893}$ alone, or Lc$_{753-893}$ together with GST SNAP-25$_{1-206}$ display slight run-down in whole-cell Ca^{2+} currents evoked by step-depolarizing voltage pulses from a holding potential of −70 to 0 mV. Cells dialyzed with GST SNAP-25$_{1-206}$ show a markedly gradual decrease in whole-cell Ca^{2+} currents with recording time. *B*: Compiled data illustrate that the intracellular application of GST SNAP-25$_{1-206}$ (n = 10) significantly inhibited whole-cell Ca^{2+} currents with recording time, as compared with the intracellular application of GST (control, n = 9), Lc$_{753-893}$ (n = 10) alone, or Lc$_{753-893}$ together with GST SNAP-25$_{1-206}$ (n = 10). Data are means ± SE. Statistical significance was evaluated by one-way ANOVA followed by least significant difference test. *P < 0.05 and **P < 0.01 vs. controls; ⋆P < 0.05 and ⋆⋆P < 0.01 vs. Lc$_{753-893}$; +P < 0.05 vs. Lc$_{753-893}$ plus GST SNAP-25$_{1-206}$.

−70 to 0 mV at 0.05 Hz. As shown in Fig. 1, whole-cell Ca^{2+} currents recorded from cells treated with GST SNAP-25$_{1-206}$ gradually and markedly decreased during recording in comparison with those from control or Lc$_{753-893}$-treated cells. Interestingly, the gradual reduction in whole-cell Ca^{2+} currents induced by the intracellular application of GST SNAP-25$_{1-206}$ was counteracted by coapplication of Lc$_{753-893}$. Furthermore, there was no significant difference in Ca^{2+} current density between control cells and cells treated with Lc$_{753-893}$ (10^{-6} mol/l) alone or Lc$_{753-893}$ (10^{-6} mol/l) together with GST SNAP-25$_{1-206}$.

Identification of L_{Ca} currents in HIT-T15 cells. To record L_{Ca} currents efficiently, Cs^+ was included in the pipette solution, and Ba^{2+} and TEA were added to the bath solution to block voltage-gated outward K^+ currents. Ba^{2+} also increased the L_{Ca} conductance. Among 140 cells (15.6 ± 0.1 pF) tested, 119 displayed inward currents in response to depolarizing pulses from a holding potential of −70 mV (Fig. 2). The peak current-voltage relationship from a control cell shows that the inward current appeared at a high voltage of −30 mV, reached the maximum at 10 mV, and reversed at ~50 mV (Fig. 2*B*). These electophysiological properties were consistent with the L_{Ca} current reported in insulin-secreting β-cells by other authors (18,19). Furthermore, the inward current was greatly enhanced by 10^{-6} mol/l Bay K8644 and blocked considerably by 10^{-6} mol/l nifedipine, which are selective L_{Ca} agonists and antagonists, respectively (Fig. 2). Bay K8644 (10^{-6} mol/l) increased the peak amplitude by 185.4 ± 19.2% (n = 6) as well as shifted the current-voltage

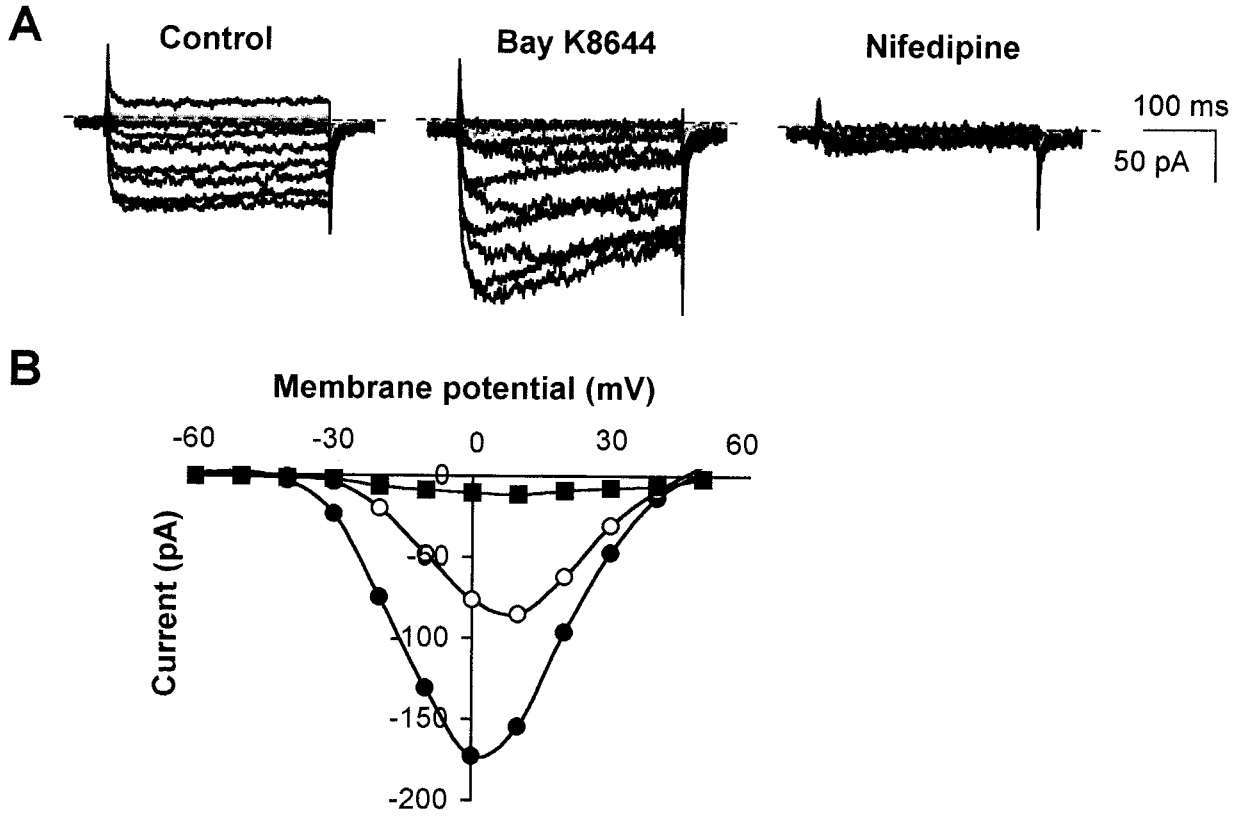

FIG. 2. Identification of L_{Ca} currents in HIT-T15 cells. ***A*****: A family of inward current traces were evoked in a HIT-T15 cell by depolarization to test pulse voltages from −60 to 50 mV for 300 ms in a 10-mV increment. The holding potential was −70 mV. Recordings were performed before (control) and after the application of 10^{-6} mol/l Bay K8644 and further application of 10^{-6} mol/l nifedipine, respectively. Dotted lines are the zero current level.** ***B*****: Current-voltage relationships obtained from a HIT-T15 cell by plotting peak inward currents against test pulse voltages before (control, ○) and after the addition of 10^{-6} mol/l Bay K 8644 (●) and further addition of 10^{-6} mol/l nifedipine (■), respectively.**

relationship to the left by 10 mV (Fig. 2*B*). In the presence of nifedipine (10^{-6} mol/l), the peak inward current amplitude was reduced to 13.7 ± 2.0% of control (n = 6). Thus, the predominant inward current (>85%) in HIT-T15 cells results from the activation of L_{CA}.

Inhibitory effect of the full-length SNAP-25 protein on L_{Ca} currents in HIT-T15 cells. To examine the effect of wild-type SNAP-25 protein on L_{Ca} currents, we introduced the full-length recombinant GST SNAP-25 protein into HIT-T15 cells via the patch pipette. This exogenously applied recombinant SNAP-25 also allows us to examine the time course of action of SNAP-25 on L_{Ca}. It has been previously shown that a protein with a molecular weight of 50 kDa can diffuse through a pipette (access resistance of 10 MΩ) into the cytosol with a time constant of 5 min (20). As shown in the lower panel of Fig. 3*A*, the inward current began to decrease from 2 min after membrane rupture in a HIT-T15 cell treated with 10^{-9} mol/l GST SNAP-25, whereas such a decline was not seen with 10^{-9} mol/l GST alone in the patch pipette (Fig. 3*A*, upper panel). The inhibition of the inward current became significant around 4 min. At 5 min, the peak inward current amplitude in GST SNAP-25–treated cells (n = 8) was reduced by 32% compared with that in GST-treated cells (n = 8, $P < 0.05$) (Fig. 3*B*). In a preliminary study, we found that GST alone (10^{-9} mol/l, n = 4) did not alter the time course of the inward current seen in control HIT-T15 cells (n = 4). Thus, cells treated with GST were used as vehicle control cells. This result indicates that SNAP-25 protein can inhibit L_{Ca} currents in HIT-T15 cells, and this is consistent with the previous finding that coexpression of SNAP-25 and L_{Ca} suppressed the Ca^{2+} currents (4). We then examined whether the inhibitory effect caused by SNAP-25 was related to its direct interaction with the cytoplasmic domain separating repeats II and III L-loop of the α1C subunit of the L_{Ca} (8) by adding both synthetic II-II L-loop (1 μmol/l $Lc_{753–893}$, a generous gift from Dr. D. Atlas, Jerusalem, Israel) and GST SNAP-25 (10^{-9} mol/l) to the pipette solution. As shown in Fig. 3*C*, SNAP-25 failed to suppress the inward current in the concomitant presence of $Lc_{753–893}$. $Lc_{753–893}$ itself had no significant effect on the inward current (Fig. 3*C*), consistent with the previous report (8). Our results indicate that $Lc_{753–893}$ blocks the binding site at SNAP-25 for the L_{Ca} and subsequently prevents the SNAP-25–induced inhibition. This was surprising for us because we previously thought that $Lc_{753–893}$ would merely extend the distance between Ca^{2+} entry through L_{Ca} and the Ca^{2+} sensing site on the insulin granule, thereby disrupting exocytosis, but would not directly affect L_{Ca} activity (8). These results suggest that interaction between SNAP-25 and the II-III L-loop of L_{Ca} is necessary for SNAP-25 to negatively modify L_{Ca} activity in HIT-T15 cells.

Domains within SNAP-25 protein have distinct effects on L_{Ca} activities. We then explored which domain within SNAP-25 protein is responsible for its modulation of L_{Ca} activities. Acute treatment with BoNT/A cleaves SNAP-25 at Gln^{197}-Arg^{198} to generate a membrane-bound

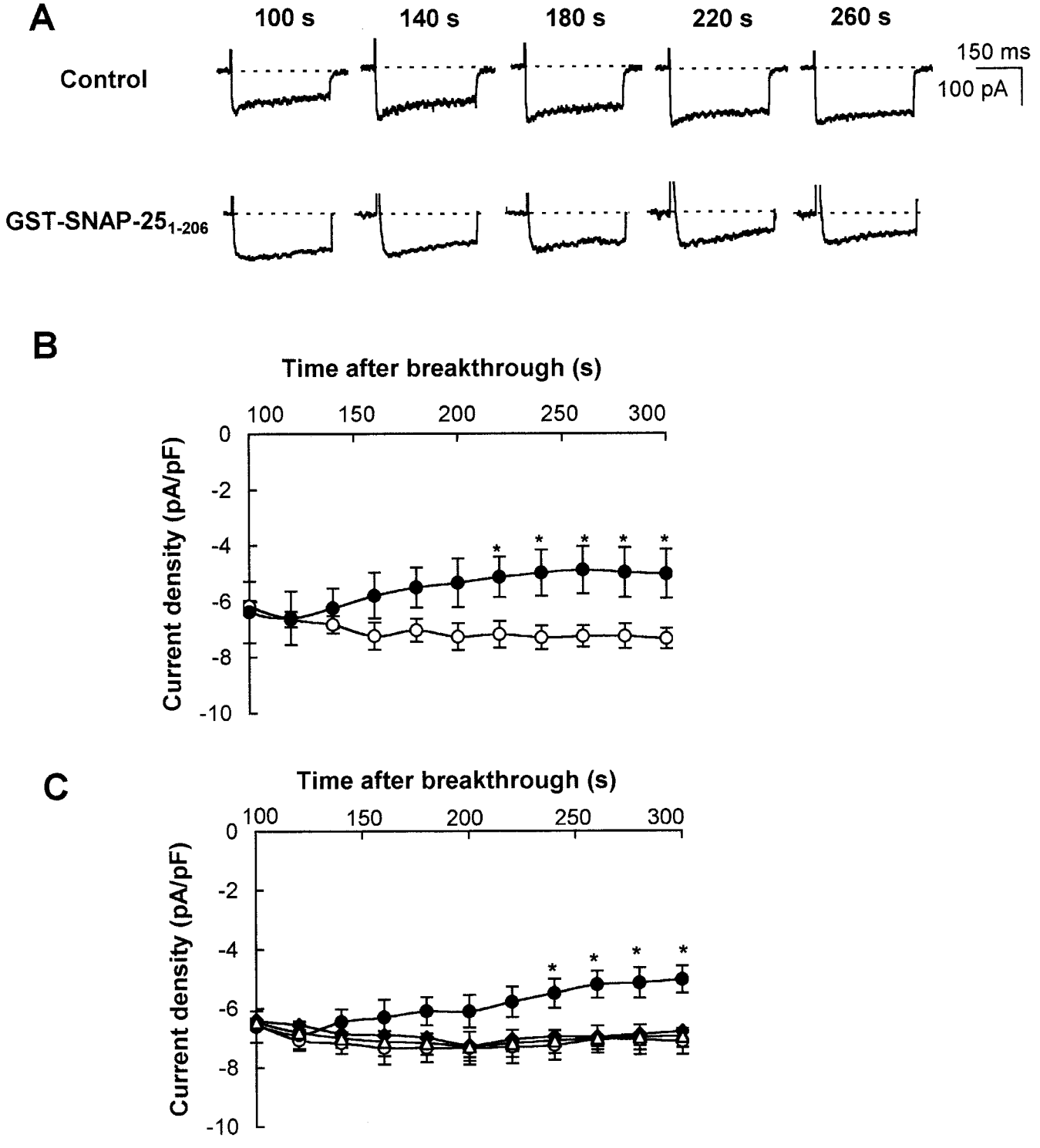

FIG. 3. Inhibitory effect of GST SNAP-25$_{1–206}$ on L_{Ca} currents in HIT-T15 cells. *A*: Representative inward currents obtained at various times after breakthrough from two HIT-T15 cells dialyzed with 10^{-9} mol/l GST (control) and 10^{-9} mol/l GST SNAP-25$_{1–206}$, respectively. Inward currents were elicited by depolarization to 10 mV for 300 ms from a holding potential of −70 mV. *B*: Peak inward currents with time from HIT-T15 cells treated with 10^{-9} mol/l GST (control, ○; $n = 8$) and 10^{-9} mol/l GST SNAP-25$_{1–206}$ (●, $n = 8$). Each point is means ± SE. *$P < 0.05$ against corresponding control data using Student's *t* test. *C*: Lc$_{753–893}$ (1 μmol/l) reversed the inhibitory effect of GST SNAP-25$_{1–206}$. Peak inward currents from HIT-T15 cells treated with 10^{-9} mol/l GST (control, ○; $n = 6$), 10^{-9} mol/l GST SNAP-25$_{1–206}$ (●, $n = 6$), 1 μmol/l Lc$_{753–893}$ plus 10^{-9} mol/l GST SNAP-25$_{1–206}$ (◆, $n = 6$), and 1 μmol/l Lc$_{753–893}$ (△, $n = 6$). Each point represents the means ± SE. *$P < 0.05$ against corresponding control data using ANOVA. Peak inward currents from each cell were normalized by cell membrane capacitance to avoid cell size variation. Dotted lines are the zero current level.

NH_2-terminal SNAP-25$_{1–197}$ fragment and a cytosolic COOH-terminal consisting of nine amino acids, SNAP-25$_{198–206}$ (11,21). These cleavage products could compete with each other and with the remaining intact SNAP-25, making it difficult to distinguish their independent actions. We therefore used the strategy of overexpressing SNAP-25 proteins and BoNT/A light chain. The overexpressed SNAP-25 proteins will be targeted to the plasma mem-

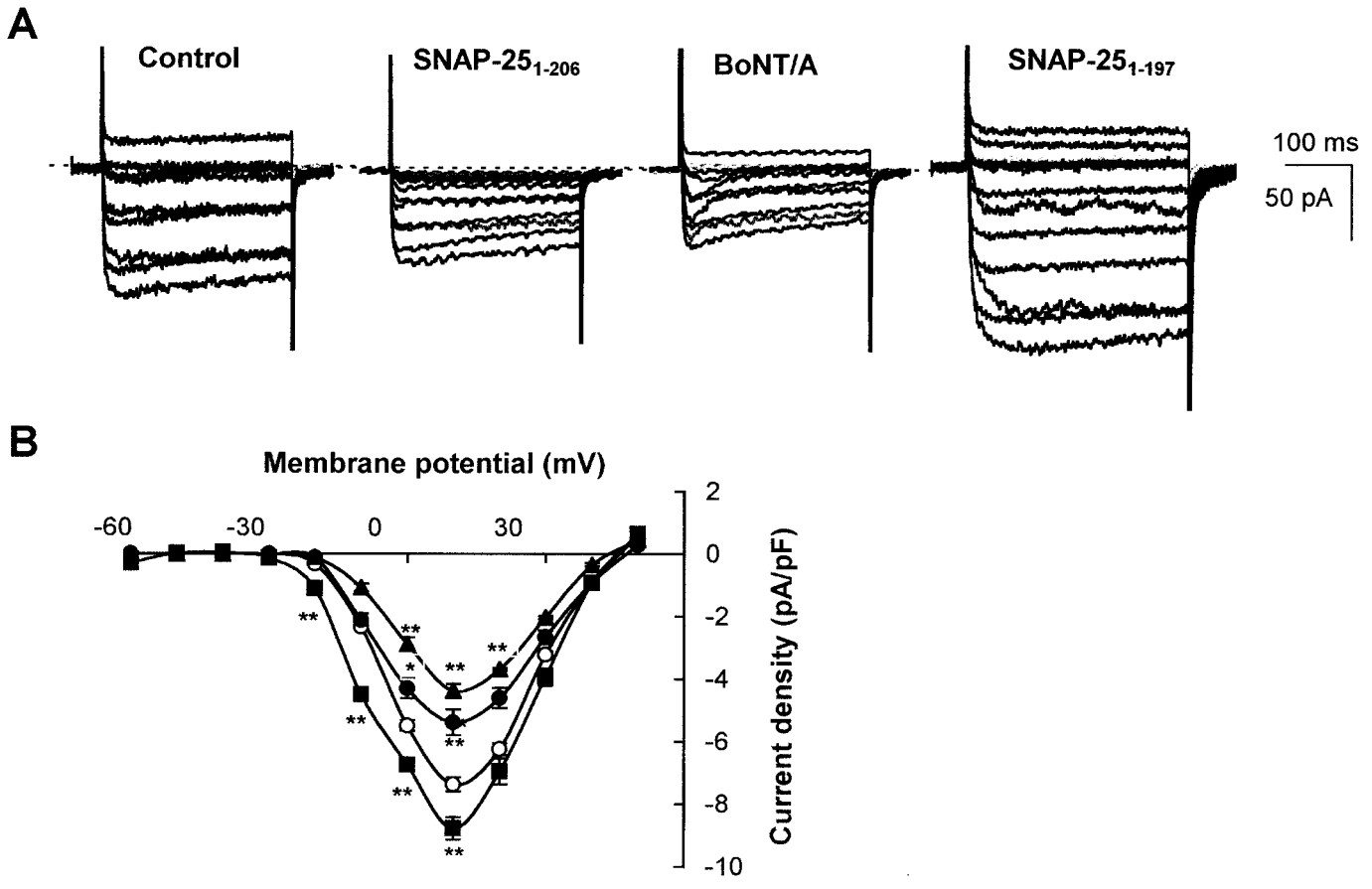

FIG. 4. Effects of different transfectants on L_{Ca} currents in HIT-T15 cells. *A*: Representative inward current traces from four HIT-T15 cells transfected with empty vector (control), SNAP-$25_{1–206}$, BoNT/A, and SNAP-$25_{1–197}$. Inward currents were evoked by depolarization from −60 to 50 mV for 300 ms from a holding potential of −70 mV. Dotted lines are the zero current level. *B*: Current-voltage curves obtained by plotting the peak inward current amplitudes against test pulse voltages. Data were normalized by cell membrane capacitance and summarized from HIT-T15 cells transfected with empty vector (control, ○; $n = 16$), SNAP-$25_{1–206}$ (●, $n = 16$), BoNT/A (▲, $n = 17$), and SNAP-$25_{1–197}$ (■, $n = 12$). Data are the means ± SE. *$P < 0.05$ and **$P < 0.01$ vs. control (ANOVA).

brane to effectively compete with endogenous SNAP-25, and the overexpressed BoNT/A will have access to all cellular SNAP-25 proteins, including those in complexes that would have cycled into uncomplexed forms. Furthermore, sufficient time for cytosolic proteolysis would deplete the cleavage products.

We first compared the effects of the overexpression of wild-type SNAP-25 (SNAP-$25_{1–206}$) and the mutant NH_2-terminal SNAP-$25_{1–197}$. Mutant SNAP-$25_{1–197}$, like SNAP-$25_{1–206}$, is capable of binding membrane syntaxin 1a (22,23), and the regions within this portion of the truncated SNAP-25 protein have been shown to directly bind to neuronal N-type Ca^{2+} (24) and neuroendocrine L_{Ca} (8). Our previous report demonstrated that transfection with wild-type SNAP-25 and mutant SNAP-$25_{1–197}$ resulted in targeting of these proteins specifically to the plasma membrane and that these SNAP-25 protein–transfected cells were identified by the coexpressed GFP (16). In a control study, the peak inward current-voltage relationship in HIT-T15 cells ($n = 4$) cotransfected with empty vectors and vectors with cDNA encoding for GFP did not show significant difference from that of untransfected cells ($n = 4$, data not shown). Therefore, those cells cotransfected with empty vectors and GFP vectors were used as control cells in all sets of experiments involving various transfectants, if not indicated otherwise. Figure 4*A* displayed the current traces evoked by voltage steps from −60 to 50 mV from four individual cells with similar membrane capacitance to minimize the cell size variation. Transfection of wild-type SNAP-25 reduced inward current amplitudes (Fig. 4*A*). Peak current-voltage relationships demonstrated that the inward currents were decreased in HIT-T15 cells expressing SNAP-25 protein in a voltage-dependent manner (Fig. 4*B*). The inhibition became significant at 0 mV, reached maximum at 10 mV, and disappeared at potential positive to 20 mV. At 10 mV, cell transfection with SNAP-$25_{1–206}$ attenuated the peak current amplitude by 27%, similar to the 31% inhibition observed in cells in which GST SNAP-$25_{1–206}$ was introduced to the cell interior via the patch pipette. The current-voltage curve, however, did not shift in any direction (Fig. 4*B*). These data further confirm that SNAP-$25_{1–206}$ protein can inhibit L_{Ca} activity in HIT-T15 cells.

However, in contrast to the wild-type SNAP-25, expression of the mutant SNAP-$25_{1–197}$ did not decrease but instead paradoxically increased the inward currents (Fig. 4*A*). Figure 4*B* shows that inward current amplitudes were significantly augmented in cells expressing SNAP-$25_{1–197}$ at membrane potentials from −20 to 10 mV. At 10 mV, overexpression of SNAP-$25_{1–197}$ increased the peak current amplitude by 19%. We next investigated whether the excitatory effect of SNAP-$25_{1–197}$ was associated with the

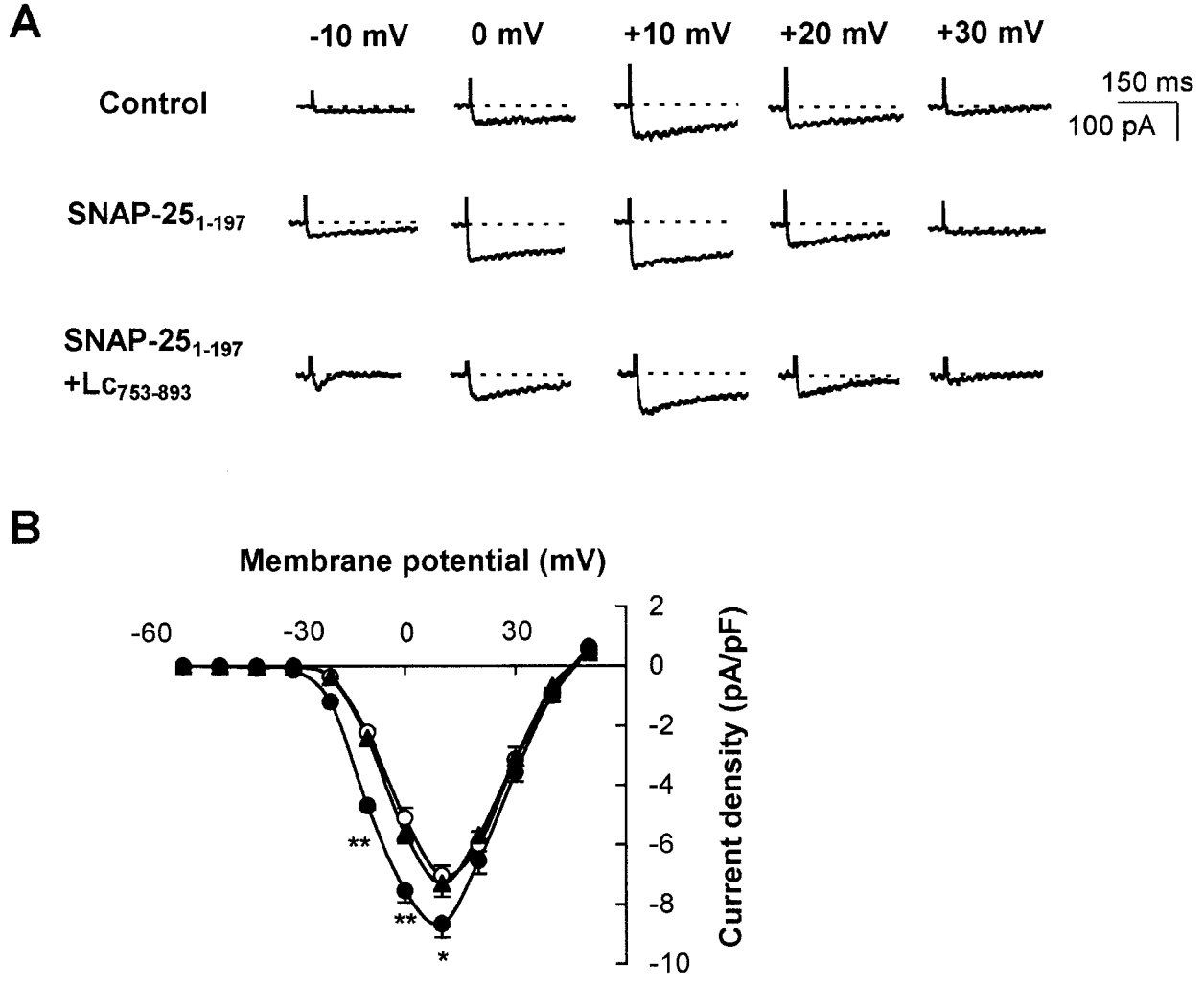

FIG. 5. Lc$_{753–893}$ reversed the stimulatory effect of SNAP-25$_{1–197}$. *A*: Representative inward current traces elicited by 300-ms depolarization to step voltages, as indicated in a control cell, a SNAP-25$_{1–197}$–transfected cell, and a SNAP-25$_{1–197}$–transfected cell dialyzed with Lc$_{753–893}$ (1 μmol/l). The holding potential was −70 mV. Dotted lines indicate the zero current level. *B*: Current-voltage curves were determined by plotting peak inward currents against step voltages in control cells (○, n = 8), SNAP-25$_{1–197}$–transfected cells (●, n = 6), and SNAP-25$_{1–197}$–transfected cells treated with Lc$_{753–893}$ (1 μmol/l) (▲, n = 6). We began to record current traces 10 min after membrane rupture to allow Lc$_{753–893}$ peptide to dialyze the cytosol sufficiently. Data are means ± SE and are normalized to cell membrane capacitance. *P < 0.05 and **P < 0.01 vs. control (ANOVA).

Lc loop of the α1C subunit. We used another set of experiments in which 1 μmol/l Lc$_{753–893}$ peptide was injected via the patch pipette into HIT-T15 cells already expressing mutant SNAP-25$_{1–197}$. The data were collected 5 min after the membrane breakthrough to allow Lc$_{753–893}$ peptides to diffuse into the cell. As shown in Fig. 5*A*, injection of the Lc$_{753–893}$ peptide blocked the stimulatory effect of SNAP-25$_{1–197}$ at potentials from −20 to 10 mV. For example, the inward current density at 10 mV was −8.7 ± 0.5 pA/pF in SNAP-25$_{1–197}$–transfected cells (n = 8, P < 0.05 vs. control) and reversed to −7.3 ± 0.5 pA/pF after injecting Lc$_{753–893}$ into SNAP-25$_{1–197}$–transfected cells (n = 7), which was close to −7.0 ± 0.3 pA/pF in control cells (n = 8) (Fig. 5*B*). Taken together, these results indicate that SNAP-25$_{1–197}$ has an opposite effect on L_{Ca} currents, as compared with SNAP-25$_{1–206}$, and that its excitatory action is also associated with direct interaction with the Lc loop of the L_{Ca}.

We then examined the effects of depletion of endogenous SNAP-25 protein by transfection with BoNT/A light chain. We predicted that because wild-type SNAP-25 inhibits L_{Ca}, its depletion by BoNT/A should relieve this inhibition. Surprisingly, Fig. 4*A* shows that transfection with BoNT/A paradoxically decreased the L_{Ca} currents to an even greater extent than wild-type SNAP-25$_{1–206}$. The current-voltage relationship demonstrated that the BoNT/A-induced inhibition was also voltage dependent, with statistical significance between 0 and 20 mV (Fig. 4*B*). At a membrane potential of 10 mV, BoNT/A inhibited the peak inward current amplitude by 41%, whereas wild-type SNAP-25$_{1–206}$ inhibited it by only 27% (Fig. 4*B*).

The greater inhibition by BoNT/A expression is likely due to absence of a tonic-positive regulatory effect of the NH_2-terminal SNAP-25$_{1–197}$ domain on L_{Ca} currents. Wild-type SNAP-25–mediated inhibition could therefore not be ascribed to this product. COOH-terminal SNAP-25$_{198–206}$ peptide, another BoNT/A cleavage product, was therefore tested for its ability to mimic the inhibitory effects of wild-type SNAP-25. As shown in Fig. 6, injecting synthetic SNAP-25$_{198–206}$ (10^{-9} mol/l) into HIT-T15 cells (n = 6) began to suppress the inward current from 5 min after membrane rupture and reached the maximum inhibition of

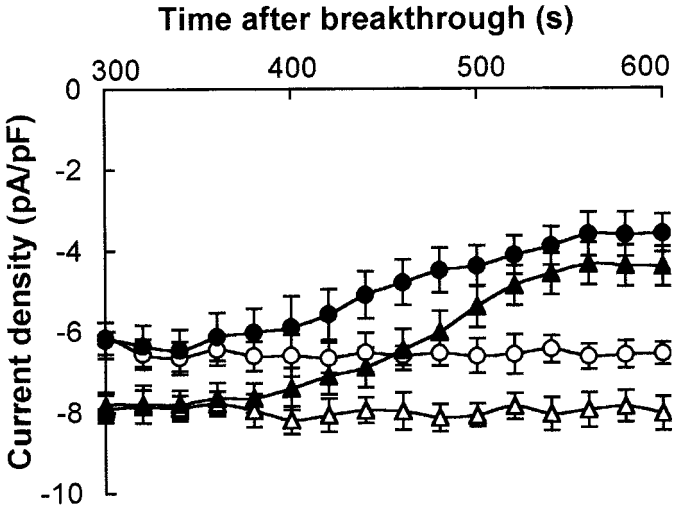

FIG. 6. Time course of SNAP-$25_{198–206}$ effect on L_{Ca} currents. Inward currents were obtained by depolarization to 10 mV from a holding potential of −70 mV. Peak inward currents with time from control HIT-T15 cells (○, n = 6), control cells dialyzed with 10^{-9} mol/l SNAP-$25_{198–206}$ (●, n = 6), SNAP-$25_{1–197}$–transfected cells (△, n = 6), and SNAP-$25_{1–197}$–transfected cells dialyzed with 10^{-9} mol/l SNAP-$25_{198–206}$ (▲, n = 6). Each point is the means ± SE. Current values were normalized to cell membrane capacitance.

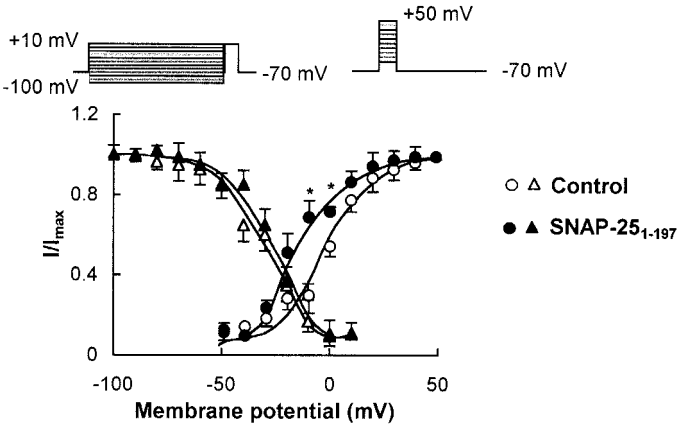

FIG. 7. Effects of mutant SNAP-$25_{1–197}$ on voltage-dependent activation and inactivation of the L_{Ca}. Voltage-dependent activation curves (protocol shown at the top right) were determined by plotting normalized peak tail current amplitudes against test pulse voltages. Smooth lines were the best fits to Boltzmann equation: $I/I\max = 1/\{1+ \exp[(V_{1/2} - V)/k]\}$, where $V_{1/2}$ is the half-maximal activation potential and k the slope factor. Values for $V_{1/2}$ and k are shown in Table 1. Data are the means ± SE from control (△, n = 12) and SNAP$25_{1–197}$–transfected (▲, n = 8) HIT-T15 cells. *$P < 0.05$ against control. For voltage-dependent inactivation curves (protocol shown at the top left), the cell membrane was first held for 15 s at various prepulse potentials between −100 and 10 mV in 10-mV increments. After a brief interval at voltage of −70 mV, the cell membrane was then depolarized to 10 mV for 200 ms to elicit inward currents. Inactivation curves were obtained by plotting normalized steady-state current amplitudes against respective prepulse voltages. Smooth curves represented the best fits to a Boltzmann equation: $I/I\max = 1/\{1+ \exp[(V - V_{1/2})/k]\}$, where $V_{1/2}$ is the half-maximal inactivation potential and k the slope factor. Values for $V_{1/2}$ (inactivation) and k are also shown in Table 1.

47% at 10 min, as compared with control cells (n = 6). Furthermore, introduction of synthetic SNAP-$25_{198–206}$ (10^{-9} mol/l) into HIT-T cells transfected with SNAP-$25_{1–197}$ also resulted in the reduction of the inward current, with a maximum inhibition of 34% occurring at 10 min after membrane rupture, as compared with control cells (Fig. 6). These data suggest that SNAP-$25_{198–206}$ is likely the putative domain within SNAP-25 that inhibits L_{Ca} currents and exerts a dominant effect over the NH_2-terminal SNAP-$25_{1–197}$ domain.

Effects of different transfections on voltage-dependent activation and inactivation of the L_{Ca}. Because L_{Ca} current amplitudes were affected by different transfections, we further explored how these transfections could affect L_{Ca} kinetics. Therefore, both voltage- and time-dependent activation and inactivation were examined in the following studies. Voltage-dependent activation curves were obtained by plotting normalized peak tail currents against test pulses. In this set of experiments, only expression of the truncated SNAP-$25_{1–197}$ in HIT-T15 cells shifted the activation curve 10 mV toward the left (Fig. 7), indicating that the L_{Ca} is easier to activate at lower voltages in the presence of SNAP-$25_{1–197}$, consistent with its stimulatory effect on this channel (Fig. 4*B*). However, transfection with SNAP-$25_{1–206}$ or BoNT/A did not affect activation kinetics (Table 1). Parameter values for voltage-dependent activation kinetics are summarized in Table 1.

Voltage-dependent inactivation of the L_{Ca} was assessed using a standard two-step protocol in which long duration prepulses (15 s) of varying test potentials were followed by a short step to 10 mV. The steady-state inward current, after the 10-mV test pulse from each prepulse, was measured as a fraction of the maximal inward current. The voltage-dependent inactivation curve was obtained by plotting these fractional values against prepulse voltages and best-fitted by the Boltzmann equation (Fig. 7). No transfections significantly altered the inactivation curve. Only control and SNAP-$25_{1–197}$ data for voltage-dependent inactivation are shown in Fig. 7. The values for voltage-dependent inactivation parameters are also summarized in Table 1.

Effects of different transfectants on time-dependent activation and inactivation of the L_{Ca}. Time constants during activation were obtained by fitting depolarization-evoked inward current traces with a mono-exponential function. Figure 8*A* shows that the inward current was activated faster in the cell transfected with SNAP-$25_{1–197}$ but almost unaffected in the cell transfected with SNAP-$25_{1–206}$ or BoNT/A. By calculation, the activation time constant was reduced from 2.8 ± 0.2 ms in control cells (n = 11) to 2.0 ± 0.1 ms in SNAP-$25_{1–197}$ ($n = 11, P < 0.05$), suggesting that SNAP-$25_{1–197}$ accelerates the activation rate of the L_{Ca}, again consistent with its stimulatory effect on this channel. The values for activation time constants were given in Table 2.

Time-dependent inactivation of the L_{Ca} was studied using a long (9 s) depolarizing pulse to 10 mV (Fig. 8*B*). Time constants (τ_1 and τ_2) of the inward current decay were calculated by fitting current traces with a biexponential equation. As shown in Table 2, SNAP-$25_{1–206}$ accelerated the inactivation rate of the L_{Ca}, with τ_1 and τ_2 increased by 1.5- and 1.6-fold, respectively, which was in agreement with the previous study performed in *Xenopus* oocyte (4). The absolute values for τ_1 were larger in our experiment. The reason for this was probably the replacement of the bath solution Ca^{2+} with Ba^{2+}, which could slow down the inactivation rate of the L_{Ca}. Transfection with BoNT/A also increased the inactivation rate, but transfection with SNAP-$25_{1–197}$ significantly decelerated it

TABLE 1
Alteration of voltage-dependent kinetics of the L_{Ca}

	Activation		Inactivation	
	$V_{1/2}$ (mV)	k (mV)	$V_{1/2}$ (mV)	k (mV)
Control	−5.0 ± 0.9 (6)	13.4 ± 0.9 (6)	−25.0 ± 2.4 (6)	11.5 ± 1.1 (6)
SNAP-$25_{1–206}$	−3.2 ± 0.6 (5)	11.2 ± 1.4 (5)	−21.6 ± 3.1 (5)	11.9 ± 0.3 (5)
BoNT/A	−2.9 ± 0.4 (5)	12.7 ± 1.5 (5)	−26.4 ± 2.6 (5)	11.6 ± 1.2 (5)
SNAP-$25_{1–197}$	−15.1 ± 1.8 (6)*	10.2 ± 1.9 (6)	−24.7 ± 1.7 (5)	11.2 ± 1.0 (5)

Data are means ± SE. The number of cells used is shown in parentheses. Definitions for $V_{1/2}$ and k are given in the legend for Fig. 7. *$P <$ 0.05 against control.

(Fig. 8*B* and Table 2). These data may therefore partially explain changes in inward current amplitudes, as seen in Fig. 4. That is, faster inactivation caused by SNAP-$25_{1–206}$ and BoNT/A results in smaller inward current amplitudes, whereas slower inactivation induced by SNAP-$25_{1–197}$ leads to larger inward current amplitudes.

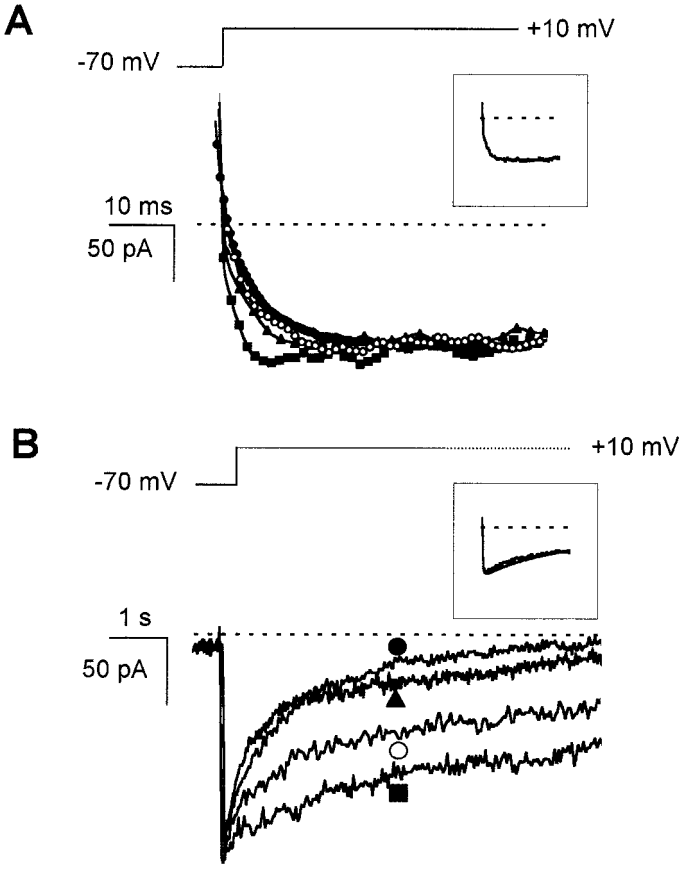

FIG. 8. Effects of different transfectants on time-dependent kinectics of the L_{Ca}. *A*: Time-dependent activation. Representative inward current traces from four HIT-T15 cells transfected with empty vector (○), SNAP-$25_{1–206}$ (●), BoNT/A (▲), and SNAP-$25_{1–197}$ (■). Inward currents were evoked in response to a test pulse of 10 mV for 300 ms from a holding potential of −70 mV and normalized to the same amplitude to compare their activation time course more efficiently. Only initial segments of current traces are displayed. The inset shows that a typical inward current was well fitted with a monoexponential curve. *B*: Time-dependent inactivation. Representative inward current traces were elicited by a 9-s test pulse to 10 mV from a holding potential of −70 mV from four cells transfected with empty vector (○), SNAP-$25_{1–206}$ (●), BoNT/A (▲), and SNAP-$25_{1–197}$ (■). Current traces were superimposed based on the same amplitude to compare their decay more conveniently. The inset shows that the inward current was well fitted with a biexponential curve. Dotted lines are the zero current level. Time constant values for activation and inactivation are shown in Table 2.

Effects of different transfectants on Ca^{2+} influx through the L_{Ca}. In pancreatic β-cells, Ca^{2+} entry through L-type channels triggers the exocytosis of insulin granules (25). Therefore, modulation of L_{Ca} channel activity by SNAP-25 proteins could consequently affect Ca^{2+} influx and cytoplasmic-free Ca^{2+} concentration ($[Ca^{2+}]_i$). To test this, we measured $[Ca^{2+}]_i$ in single HIT-T15 cells using Fura 2 as Ca^{2+} indicator. The HIT-T15 cells studied were transfected with the empty vector (control), SNAP-$25_{1–206}$, BoNT/A, or SNAP-$25_{1–197}$. Transfection was again determined by coexpression of GFP in each experiment. HIT-T15 cells were placed in a 1-ml chamber with Ca^{2+}-containing physiological solution (see RESEARCH DESIGN AND METHODS). After the basal $[Ca^{2+}]_i$ level was recorded, the cells were treated with 10 mmol/l KCl, which depolarizes the cell membrane and subsequently activates L_{Ca}. The difference between the peak transient rise in $[Ca^{2+}]_i$ and the basal $[Ca^{2+}]_i$ was considered as net Ca^{2+} influx through L_{Ca}. To minimize the possible inter- and intra-assay variations, $[Ca^{2+}]_i$ values from cells (usually 3–4) with efficient transfection in each field were averaged, and only one field was counted from each chamber. Figure 9*A* shows that expression of SNAP-$25_{1–206}$ and BoNT/A in HIT-T15 cells decreased the peak transient rise in $[Ca^{2+}]_i$, whereas SNAP-$25_{1–197}$ had an opposite effect. Data for the peak transient rise in $[Ca^{2+}]_i$ were averaged in Fig. 9*B*. In control cells, the peak transient rise in $[Ca^{2+}]_i$ was 199.1 ± 10.4 nmol/l ($n = 6$). SNAP-$25_{1–206}$ and BoNT/A reduced it to 150.6 ± 5.4 nmol/l ($n = 6$, $P < 0.05$) and 134.1 ± 7.8 nmol/l ($n = 6$, $P < 0.05$), respectively, whereas SNAP-$25_{1–197}$ raised it to 248.1 ± 18.1 nmol/l ($n = 6$, $P < 0.05$). These data, therefore, are in agreement with our L_{Ca} current recordings (Fig. 4) and provide further evidence that domains within SNAP-25 protein have distinct effects on the L_{Ca}.

DISCUSSION

In this study, we demonstrate for the first time that SNAP-25 specifically modulates L_C subtype Ca^{2+} channel activity in insulin-secreting cells. This indicates that SNAP-25 not only functions as a key component in a core complex to trigger insulin exocytosis but also interacts with the voltage-gated L_{Ca} to control Ca^{2+} influx, which plays an important role in the formation of the core complex (4,8). The degree of inhibition of full-length SNAP-25 on whole-cell Ca^{2+} currents in the primary pancreatic β-cell was smaller than that observed in the HIT-T15 cell. This is probably due to the relative small contribution of the L_C subtype Ca^{2+} channel to the total L-type Ca^{2+} currents in normal β-cells. The predominant

TABLE 2
Alteration of time-dependent kinetics of the L_{Ca}

	Activation	Inactivation	
	τ (ms)	τ_1 (ms)	τ_2 (ms)
Control	2.8 ± 0.2 (11)	6,096.0 ± 505.2 (6)	436.2 ± 27.4 (6)
SNAP-$25_{1–206}$	2.9 ± 0.3 (11)	4,127.6 ± 280.2 (6)*	267.0 ± 36.9 (6)*
BoNT/A	2.6 ± 0.4 (11)	4,245.7 ± 273.9 (6)*	245.6 ± 30.1 (6)*
SNAP-$25_{1–197}$	2.0 ± 0.1 (11)*	9,886.6 ± 1,028.2 (6)†	464.9 ± 47.9 (6)

Data are means ± SE. The number of cells used is given in parentheses. *$P < 0.05$ and †$P < 0.01$ vs. control.

subtype of the L_{Ca} in islet β-cells is the L_D subtype (26–28), whereas HIT-T15 cells predominantly contain the L_C subtype. These results also suggest that although the L_C and L_D subtypes of L_{Ca} share a 70% homology (29), the L_C subtype appears to be more sensitive to SNAP-25. In contrast, syntaxin 1A appears to similarly inhibit both the L_C and L_D subtypes of β-cell L_{Ca} (4,8,28).

We also present the first evidence that domains within the SNAP-25 protein are capable of causing distinct changes in L_{Ca} kinetics. Wild-type SNAP-25 reduced the inward current amplitude and accelerated its inactivation rate, indicating its inhibitory regulatory role on the L_{Ca}, which is consistent with the previous report (4). It is likely that SNAP-$25_{1–206}$ acts on the inactivation state of the channel and results in its faster decay. However, BoNT/A expression, which depleted all cellular SNAP-25 proteins, resulted in an even greater inhibition of L_{Ca} currents. Specifically, BoNT/A expression decreased the current

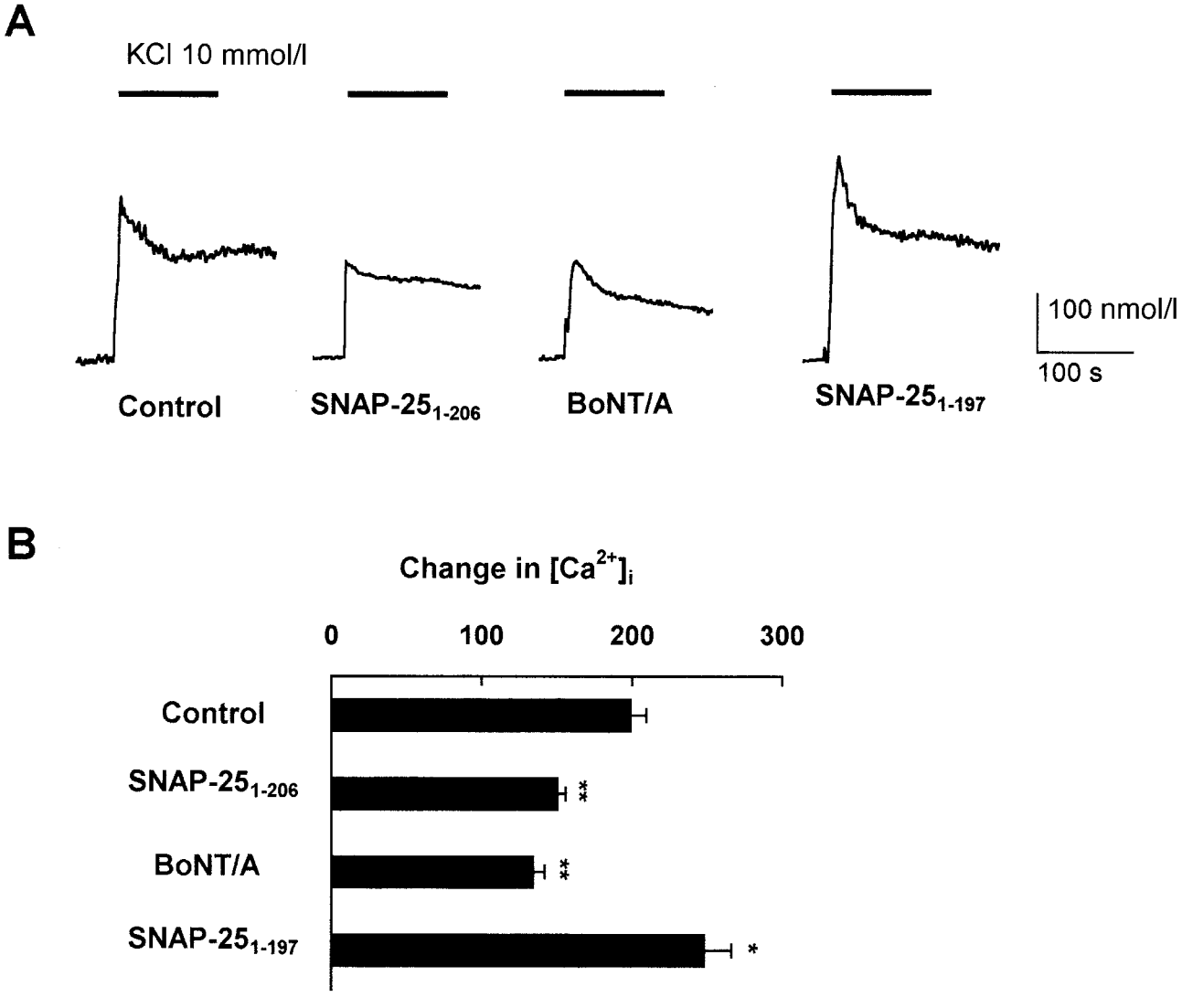

FIG. 9. Effects of different transfectants on $[Ca^{2+}]_i$ in HIT-T15 cells. *A*: Transient rise in $[Ca^{2+}]_i$ in response to 10 mmol/l KCl from HIT-T15 cells transfected with empty vector, SNAP-$25_{1–206}$, BoNT/A, and SNAP-$25_{1–197}$. *B*: Peak transient rise in $[Ca^{2+}]_i$ summarized from control ($n = 6$), SNAP-$25_{1–206}$–transfected ($n = 6$), BoNT/A-transfected ($n = 6$), and SNAP-$25_{1–197}$–transfected ($n = 6$) HIT-T15 cells, respectively. Each bar is the means ± SE. *$P < 0.05$ against control (ANOVA); **$P < 0.01$.

amplitude, accelerated the inactivation rate, and reduced the Ca^{2+} influx. BoNT/A expression has the advantage over the acute application of BoNT/A. The latter could acutely generate cleavage products that compete with each other and with the remaining intact SNAP-25, therefore preventing assessment of the independent effect of the functional domains within SNAP-25. The greater inhibition observed with BoNT/A expression suggests that SNAP-25 contains not only negative but also positive regulatory domains. Indeed, we found the COOH-terminal SNAP-$25_{198–206}$ peptide to confer the inhibitory effect of SNAP-25 and of BoNT/A, whereas the membrane-bound NH_2-terminal SNAP-$25_{1–197}$ conferred a paradoxical stimulatory effect on the L_{Ca}. The fact that COOH-terminal SNAP-$25_{198–206}$ peptide is able to override the positive regulatory effect of SNAP-$25_{1–197}$ indicates that the negative regulatory role of SNAP-25 on the L_{Ca} probably predominates in the islet β-cell. Nonetheless, this dominant-negative regulatory effect of SNAP-25 is balanced by the positive regulatory domain, as evidenced by its complete absence effected by BoNT/A transfection, which caused an even greater inhibition of the Ca^{2+} channel than the SNAP-25 overexpression. It therefore seems likely that both negative and positive regulatory domains of the SNAP-25 protein are operative in modulating the Ca^{2+} channel in the islet β-cell.

SNAP-$25_{1–197}$ increased the current amplitude (Fig. 4), activated L_{Ca} at lower membrane potentials (Fig. 7), and decelerated its inactivation rate (Fig. 8*B*). These results indicate that SNAP-$25_{1–197}$ may interact with more than one site at the L_{Ca}. Injecting the $Lc_{753–893}$ peptide into HIT cells transfected with SNAP-$25_{1–197}$ or wild-type SNAP-$25_{1–206}$ restored the current-voltage curve to control levels, indicating that both SNAP-25 proteins modulated the L_{Ca} by direct interaction with the channel. This is further supported by the previous study showing a direct binding between SNAP-25 and L_{Ca} (8). Nonetheless, wild-type SNAP-25 and mutant SNAP-$25_{1–197}$ must be bound to the II-III L-loop of L_{Ca} in distinct conformations to assert these apparent opposite effects on L_{Ca} and the resulting Ca^{2+} influx (Fig. 9). In our previous report, where data collected were from a field of both transfected and untransfected cells (transfection efficiency ~45%), we did not observe an obvious difference in KCl-evoked Ca^{2+} influx between SNAP-$25_{1–197}$– and wild-type SNAP-25–transfected cells (16). However, in the current study, data were collected from cells with the highest protein expression, as determined by GFP coexpression, therefore permitting the effects to be seen. Despite its positive modification of the L_{Ca}, overexpression of SNAP-$25_{1–197}$ caused a net inhibition of insulin secretion in HIT-T15 cells (16), likely due to the formation of nonfunctional exocytotic SNARE complexes (22,23).

Injection of the COOH-terminal SNAP-$25_{198–206}$ inhibited L_{Ca} currents to a greater extent than wild-type SNAP-25, and interestingly, these inhibitory effects dominated over the stimulatory effects of SNAP-$25_{1–197}$ expression. The greater inhibition by overexpression of BoNT/A over the wild-type SNAP-25 further supports our hypothesis that these two domains of SNAP-25, NH_2-terminal SNAP-$25_{1–197}$, and COOH-terminal SNAP-$25_{198–206}$ exert a "yin yang" effect on the L_{Ca}. This might in part explain why the presence of higher levels of extracellular Ca^{2+} or higher membrane depolarization could abrogate the inhibitory effects of the acutely applied BoNT/A (13,15), wherein the COOH-terminal SNAP-$25_{198–206}$, which initially blocks the L_{Ca}, binds insulin granule VAMP-2 to form a nonfunctioning fusion complex (16). However, its subsequent accelerated proteolysis in the cytosol would leave the relatively intact membrane-bound SNAP-$25_{1–197}$ unopposed to act on the L_{Ca} to increase Ca^{2+} influx. Whereas SNAP-$25_{1–197}$ also forms a nonfunctional docking complex (16), the increased Ca^{2+} influx might overcome this inhibition. In support, Coorssen et al. (30) demonstrated that increased Ca^{2+} levels could effect exocytosis independent of the SNARE complex and that the latter may serve to modulate Ca^{2+} sensitivity in driving fusion. Furthermore, in contrast to a neuron that has a higher proportion of secretory granules in a readily releasable pool of docked vesicles (~10%), <4% of insulin secretion granules in β-cells are in this pool (25,31). The vast majority of insulin granules are located more distantly from the membrane, within a reserve pool. The initial phase of $[Ca^{2+}]_i$ rise is important for exocytosis of the readily releasable pool (32,33), whereas the subsequent sustained elevation of $[Ca^{2+}]_i$ acts to prime and mobilize the reserve pool to the readily releasable pool (32,33). The SNAP-$25_{1–197}$ stimulatory effects on the L_{Ca} may compensate for the reduced insulin exocytosis caused by the nonfunctional docking complex by mobilizing more secretion granules from the reserve pool to the readily releasable pool.

Taken together, we have now provided evidence that domains within SNAP-25 protein have distinct effects on the L_{Ca}. These results have the potential to elucidate how SNARE proteins may not only regulate physiological insulin exocytosis but also be of pathophysiological significance in the dysregulation of Ca^{2+} influx–mediated islet β-cell injury in diabetes (1–3). In fact, SNARE protein expression levels were diminished in islets of type 2 diabetic models, including Zucker *fa/fa* and GK rats (34,35), which exhibit abnormal regulation of Ca^{2+} influx and insulin exocytosis (36). Reconstitution of these SNARE proteins, particularly SNAP-25 and syntaxin, partially restored insulin secretion to normal levels (35), likely by restoring the diabetic dysregulation of the distal components of the insulin exocytotic machinery, in particular the L_C excitosome. Finally, the positive regulatory domains within these SNARE proteins, particularly within the NH_2-terminal SNAP-$25_{1–197}$ protein, could serve as targets for novel drug design to treat diabetes.

ACKNOWLEDGMENTS

This work was supported by grants to H.Y.G. from the Canadian Diabetes Association and the Canadian Institutes for Health Research as well as grants from the National Institutes of Health (DK55160) and Juvenile Diabetes Research Foundation. Support for this work was also obtained from grants from the Swedish Medical Research Council, the Swedish Diabetes Association, the Nordic Insulin Foundation Committee, the Fredrik and Ingrid Thurings Foundation, Funds of Karolinska Institutet, the Berth von Kantzows Foundation, the Novo Nordisk

Foundation, the Swedish Society of Medicine, and the Swedish National Board of Health and Welfare.

We thank Daphne Atlas, Robert Tsushima, Eva Pasyk, and Anne Marie Salapatek for their critical review of the manuscript and technical advice.

REFERENCES

1. Juntti-Berggren L, Larsson O, Rorsman P, Ammala C, Bokvist K, Wahlander K, Nicotera P, Dypbukt J, Orrenius S, Hallberg A, Berggren PO: Increased activity of L-type Ca^{2+} channels exposed to serum from patients with type 1 diabetes. *Science* 261:86–90, 1993
2. Efanova IB, Zaitsev SV, Zhivotovsky B, Kohler M, Efendic S, Orrenius S, Berggren PO: Glucose and tolbutamide induce apoptosis in pancreatic beta-cells: a process dependent on intracellular calcium concentration. *J Biol Chem* 273:33501–33507, 1998
3. Wang L, Bhattacharjee A, Zuo Z, Hu F, Honaknen RE, Berggren PO, Li M: A low voltage-activated Ca^{2+} current mediates cytokine-induced pancreatic b-cell death. *Endocrinology* 140:1200–1204, 1999
4. Wiser O, Bennet MK, Atlas D: Functional interaction of syntaxin and SNAP-25 with voltage-sensitive L- and N-type Ca^{2+} channels. *EMBO J* 15:4100–4110, 1996
5. Bezprozvanny I, Scheller RH, Tsien RW: Functional impact of syntaxin on gating of N-type and Q-type calcium channels. *Nature* 378:623–626, 1995
6. Sheng Z-H, Rettig J, Cook T, Catterall WA: Calcium-dependent interaction of N-type calcium channels with the synaptic core complex. *Nature* 379:451–454, 1996
7. Bokvist K, Eliasson L, Ammala C, Renstrom E, Rorsman P: Co-localization of L-type calcium channels and insulin-containing secretory granules and its significance for the initiation of exocytosis in mouse pancreatic β cells. *EMBO J* 14:50–57, 1995
8. Wiser O, Trus M, Hernandez A, Renstrom E, Barg S, Rorsman P, Atlas D: The voltage sensitive Lc-type Ca^{2+} channel is functionally coupled to the exocytotic machinery. *Proc Natl Acad Sci U S A* 96:248–253, 1999
9. Sudhof TC: The synaptic vesicle cycle: a cascade of protein-protein interactions. *Nature* 375:645–653, 1995
10. Niemann H, Blasi J, Jahn R: Clostridial neurotoxins: new tools for dissecting exocytosis. *Trends Cell Biol* 4:179–185, 1994
11. Binz T, Blasi J, Yamasaki S, Baumeister A, Link E, Sudhof TC, Jahn R, Niemann H: Proteolysis of SNAP-25 by types E and A botulinal neurotoxins. *J Biol Chem* 269:1617–1620, 1994
12. Wheeler MB, Sheu L, Ghai M, Bouquillon A, Grondin G, Weller U, Beaudoin AR, Bennett MK, Trimble WS, Gaisano HY: Characterization of SNARE protein expression in β cell lines and pancreatic islets. *Endocrinology* 137:1340–1348, 1996
13. Sadoul S, Lang J, Montecucco C, Weller U, Regazzi R, Catsicas S, Wolljeim CB, Halban PA: SNAP-25 is expressed in islets of Langerhans and is involved in insulin release. *J Cell Biol* 128:1019–1028, 1995
14. Lang J, Zhang H, Vaidyanathan V-V, Sadoul K, Niemann H, Wollheim CB: Transient expression of botulinum neurotoxin C1 light chain differentially inhibits calcium and glucose induced insulin secretion in clonal βcells. *FEBS Lett* 419:13–17, 1997
15. Xu T, Binz T, Niemann H, Neher E: Multiple kinetic components of exocytosis distinguished by neurotoxin sensitivity. *Nature Neurosci* 1:192–200, 1998
16. Huang X, Wheeler MB, Kang Y-H, Sheu L, Lukacs GL, Trimble WS, Gaisano HY: Truncated SNAP-25 (1–197), like botulinum neurotoxin A, can inhibit insulin secretion from HIT-T15 insulinoma cells. *Mol Endo* 12:1062–1070, 1998
17. Grynkiewicz G, Poenie M, Tsien RY: A new generation of Ca^{2+} indicators with greatly improved fluorescence properties. *J Biol Chem* 260:3440–3450, 1985
18. Rorsman P, Trube G: Calcium and delayed potassium currents in mouse pancreatic β-cells under voltage-clamp conditions. *J Physiol* 374:531–550, 1986
19. Satin S, Cook L: Evidence for two calcium currents in insulin-secreting cells. *Pflügers Arch* 411:401–409, 1988
20. Pusch M, Neher E: Rates of diffusional exchange between small cells and a measuring patch pipette. *Pflügers Arch* 411:204–211, 1988
21. Blasi J, Chapman ER, Link E, Binz T, Yamasaki S, DeCamilli P, Sufhof TC, Niemann H, Jahn R: Botulinum neurotoxin A selectively cleaves the synaptic protein SNAP-25. *Nature* 365:160–163, 1993
22. Hayashi T, McMahon H, Yamasaki S, Binz T, Hata Y, Sudhof TC, Niemann H: Synaptic vesicle membrane fusion complex: action of clostridial neurotoxins on assembly. *EMBO J* 13:5051–5061, 1994
23. Pelligrini L, O'Connor VO, Lottspeich F, Betz H: Clostridial neurotoxins compromise the stability of a low energy SNARE complex mediating NSF activation of synaptic vesicle fusion. *EMBO J* 14:4705–4713, 1995
24. Seagar M, Takahashi M: Interactions between presynaptic calcium channels and proteins implicated in synaptic vesicle trafficking and exocytosis (Review). *J Bioenerg Biomembr* 30:347–356, 1998
25. Rorsman P: The pancreatic beta-cell as a fuel sensor: an electrophysiologist's viewpoint. *Diabetologia* 40:487–495, 1997
26. Iwashima Y, Pugh W, Depaoli AM, Takeda J, Seino S, Bell GI, Polonsky KS: Expression of calcium channel mRNAs in rat pancreatic islets and downregulation after glucose infusion. *Diabetes* 42:948–955, 1993
27. Seino S, Chen L, Seino M, Blondel O, Takeda, Johnson JH, Bell GI: Cloning of the alpha 1 subunit of a voltage-dependent calcium channel expressed in pancreatic beta cells. *Proc Natl Acad Sci U S A* 89:584–588, 1992
28. Yang S-N, Larsson O, Branstrom R, Bertorello AM, Leibiger B, Leibiger IB, Moede T, Kohler M, Meister B, Berggren PO: Syntaxin 1 interacts with the L_D subtype of voltage-gated Ca^{2+} channels in pancreatic βcells. *Proc Natl Acad Sci U S A* 96:10164–10169, 1999
29. Dolphin AC: Voltage-dependent calcium channels and their modulation by neurotransmitters and G proteins. *Exp Physiol* 80:1–36, 1995
30. Coorssen JR, Blank PS, Tahara M, Zimmerberg J: Biochemical and functional studies of cortical vesicle fusion: the SNARE complex and Ca^{2+} sensitivity. *J Cell Biol* 143:1845–1857, 1998
31. Renstrom E, Eliasson L, Rorsman P: Protein kinase A-dependent and -independent stimulation of exocytosis by cAMP in mouse pancreatic βcells. *J Physiol* 502:105–118, 1997
32. Chow RH, Klingauf J, Neher N: Time course of calcium concentration triggering exocytosis in neuroendocrine cells. *Proc Natl Acad Sci U S A* 91:12765–12769, 1994
33. Eliasson L, Renstrom E, Ding WG, Proks P, Rorsman P: Rapid ATP-dependent priming of secretory granules precedes Ca^{2+}-induced exocytosis in mouse pancreatic B-cells. *J Physiol* 503:399–412, 1997
34. Chan CB, MacPhail RM, Sheu L, Wheeler M, Gaisano HY: β-cell hypertrophy in *fa/fa* rats is associated with basal glucose hypersensitivity and reduced SNARE protein expression. *Diabetes* 48:997–1005, 1999
35. Nagamatsu S, Nakamichi Y, Yamamura C, Matsushima S, Watanabe T, Ozawa S, Furukawa H, Ishida H: Decreased expression of t-SNARE syntaxin 1 and SNAP25 in pancreatic beta cells is involved in impaired insulin secretion from diabetic GK rat islets: restoration of decreased t-SNARE proteins improves impaired insulin secretion. *Diabetes* 48:2367–2373, 1999
36. Okamoto Y, Ishida H, Tsuura Y, Yasuda K, Kato S, Matsubara H, Nishimura M, Mizuno H, Ikeda H, Seino Y: Hyperresponse in Ca^{2+}-induced insulin release from electrically permeabilized pancreatic islets of diabetic GK rats and its defective augmentation by glucose. *Diabetologi*a 38:772–778, 1995